ICAM-1 orchestrates the abscopal effect of tumor radiotherapy

Yang Zhao[a,1], Ting Zhang[a,1], Yanpu Wang[a], Dehua Lu[a], Jinhong Du[a], Xun Feng[a], Haoyi Zhou[a], Ning Liu[a], Hua Zhu[b], Shangbin Qin[c], Chenxin Liu[a], Xianshu Gao[c], Zhi Yang[b], and Zhaofei Liu[a,d,2]

[a]Medical Isotopes Research Center, Department of Radiation Medicine, School of Basic Medical Sciences, Peking University Health Science Center, Beijing 100191, China; [b]Key Laboratory of Carcinogenesis and Translational Research (Ministry of Education/Beijing), Department of Nuclear Medicine, Peking University Cancer Hospital and Institute, Beijing 100142, China; [c]Department of Radiation Oncology, Peking University First Hospital, Beijing 100034, China; and [d]State Key Laboratory of Natural and Biomimetic Drugs, Peking University, Beijing 100191, China

Edited by Rakesh K. Jain, Massachusetts General Hospital, Boston, MA, and approved February 16, 2021 (received for review May 22, 2020)

Compelling evidence indicates that radiotherapy (RT) has a systemic inhibitory effect on nonirradiated lesions (abscopal effect) in addition to the ablation of irradiated tumors. However, this effect occurs only in rare circumstances in clinical practice, and mechanisms underlying the abscopal effect of RT are neither fully understood nor therapeutically utilized. Here we identified that intercellular adhesion molecule-1 (ICAM-1), an inducible glycoprotein of the immunoglobulin superfamily, is up-regulated in nonirradiated tumors responsive to RT. ICAM-1 expression in preclinical animal models can be noninvasively detected by optical imaging and positron emission tomography (PET) using near-infrared fluorescence dye- and ^{64}Cu-labeled imaging probes that we synthesized, respectively. Importantly, the expression levels of ICAM-1 determined by quantitative PET imaging showed a strong negative linear correlation with the growth of nonirradiated tumors. Moreover, genetic or pharmacologic up-regulation of ICAM-1 expression by either an intratumoral injection of engineered recombinant adenovirus or systemic administration of a Toll-like receptor 7 agonist-capsulated nanodrug could induce markedly increased abscopal responses to local RT in animal models. Mechanistic investigation revealed that ICAM-1 expression can enhance both the activation and tumor infiltration of $CD8^+$ T cells to improve the responses of the nonirradiated tumors to RT. Together, our findings suggest that noninvasive PET imaging of ICAM-1 expression could be a powerful means to predict the responses of nonirradiated tumors to RT, which could facilitate the exploration of new combination RT strategies for effective ablation of primary and disseminated lesions.

positron emission tomography | radiotherapy | abscopal effect | ICAM-1 | Toll-like receptor

Radiotherapy (RT) with curative or palliative intent is routinely prescribed for the treatment of localized tumors or isolated metastasis by inducing DNA damage in tumor cells (1, 2). In addition to local antitumor effects, RT may also induce inhibition of nonirradiated or metastatic lesions outside of the radiation field, a phenomenon known as the "abscopal effect" (3). The mechanism underlying the abscopal effect of RT is currently not well elucidated, but theories suggest that it may be related to the fact that RT is capable of improving T cell priming by increasing the local availability of tumor-associated antigens (TAAs) or by driving the release of immunostimulatory cytokines (4, 5). Unfortunately, the abscopal effect of RT has been observed only rarely in clinical settings (2, 6, 7).

To augment the occurrence of the abscopal effect, a combination of RT with immunotherapy was proposed to modulate systemic immune responses (2, 8), as recent studies reported that improved abscopal effects of RT were observed when RT was combined with adjuvant granulocyte macrophage colony-stimulating factor (GM-CSF) (9) or immune checkpoint inhibitors (10–13). However, the response rates for these combination strategies remain low and are likely affected by various factors, such as radiation dose, fractionation, delivery schedules, and rational combinations (2). Therefore, unravelling the determinants of the abscopal effect is key, as this will not only broaden the understanding of its rare clinical occurrence, but also yield new avenues for combination therapies. Thus far, no effective method has been developed for detecting and predicting the abscopal response to RT (14).

In recent decades, molecular imaging approaches, such as positron emission tomography (PET), single-photon emission computed tomography (SPECT), and near-infrared fluorescence (NIRF) imaging, have emerged as robust tools for the noninvasive prediction or monitoring of tumor response at the earliest stages by quantitatively measuring biomarkers associated with tumor initiation or progression (15). In this regard, noninvasive imaging of key biomarkers associated with the occurrence of the abscopal effect may enable early prediction of antitumor efficacy, patient stratification, and guidance for combination RT therapeutic design.

In the present study, we used quantitative proteomic analysis to globally profile altered protein expression in nonirradiated tumors with an observed abscopal effect induced by local RT to the primary tumor. We further identified that intercellular adhesion molecule-1 (ICAM-1) was markedly up-regulated in these nonirradiated tumors that were responsive to RT. ICAM-1 is an inducible glycoprotein of the immunoglobulin (Ig) superfamily

Significance

Although RT serves as a frontline therapy for more than 50% of patients with malignancies, its efficacy is limited to localized tumors. Efforts in harnessing the abscopal effect of RT could systemically eliminate metastatic lesions disseminated beyond the radiation field; however, success has been limited thus far, owing to an inadequate understanding of the underlying mechanisms and an absence of reliable biomarkers for early prediction. Here we demonstrate that noninvasive PET imaging of ICAM-1 expression confers predictive value for abscopal effect efficacy at an early stage. This strategy may also facilitate potential high-throughput screening of current or novel drugs to be used in combination with RT to achieve desired antitumor therapeutic outcomes that eliminate both primary and metastatic lesions.

Author contributions: Z.L. supervised the project; Y.Z., T.Z., and Z.L. designed research; Y.Z., T.Z., Y.W., D.L., J.D., X.F., H. Zhou, N.L., H. Zhu, S.Q., C.L., X.G., and Z.Y. performed research; H. Zhu, S.Q., X.G., and Z.Y. contributed new reagents/analytic tools; Y.Z., T.Z., Y.W., and Z.L. analyzed data; and Y.Z., T.Z., and Z.L. wrote the paper.

The authors declare no competing interest.

This article is a PNAS Direct Submission.

[1]Y.Z. and T.Z. contributed equally to this work.

[2]To whom correspondence may be addressed. Email: liuzf@bjmu.edu.cn.

This article contains supporting information online at https://www.pnas.org/lookup/suppl/doi:10.1073/pnas.2010333118/-/DCSupplemental.

Published March 30, 2021.

that contains five distinct Ig-like domains, a transmembrane domain, and a short cytoplasmic tail that is expressed primarily in endothelial cells and leukocytes (16–18); however, its role in the abscopal effect induced by RT is unknown. Given the high expression of ICAM-1 in tumors showing the abscopal effect, we hypothesized that ICAM-1 could be a potential biomarker for tumors demonstrating the abscopal effect in response to RT. Thus, we assessed whether noninvasive imaging of ICAM-1 expression using specific imaging probes could predict the abscopal effect induced by RT and explored the potential mechanism by which ICAM-1 orchestrates abscopal responses. Moreover, we further investigated whether pharmacologic up-regulation of ICAM-1 expression by systemic administration of a clinically promising nanodrug could boost the abscopal effect of RT for the improved management of tumors with both primary and metastatic lesions.

Results

Quantitative Proteomic Analysis Indicates that ICAM-1 Is a Potential Indicator of the RT-Induced Abscopal Effect. To investigate whether RT can affect protein expression in tumors showing the abscopal effect at an early stage, we performed quantitative proteomic analysis in a 4T1 mouse breast cancer model (Fig. 1 *A* and *B*). BALB/c mice were inoculated with a primary tumor (irradiated tumor) and a secondary tumor (nonirradiated tumor) to mimic the primary tumor and metastatic lesions in a clinical scenario (19, 20). Because RT alone rarely induces an abscopal effect in preclinical or clinical studies (2, 21), we artificially defined "responsive" and "nonresponsive" by a relatively low criterion to better explore biomarkers in the early treatment stage. RT-treated mice were divided into responder and nonresponder groups based on the percentage change in tumor volume between days 0 and 7 of the nonirradiated tumors (Fig. 1*A*), while tumors in mice without RT were defined as the control group (Fig. 1*B*). Using this definition, we identified three responders that had significantly lower tumor volumes compared with the nonresponder and control groups ($P < 0.05$; Fig. 1*C*).

For further proteomic analysis, bilateral tumors from responder and nonresponder mice were separated into single-tumor groups based on their irradiation status: responder-nonirradiated tumor (NIT), responder-irradiated tumor (IT), nonresponder-NIT, and nonresponder-IT. Proteins identified with at least two unique peptides were quantified using the MaxLFQ algorithm (Fig. 1*D*). Using the criteria of a fold change >2.5 and false discovery rate (FDR)-adjusted P value <0.05 compared with the untreated tumors (i.e., tumors in the control group), we identified proteins that were significantly and differentially expressed (Dataset S1). Significantly up-regulated and down-regulated proteins are shown in Fig. 1*E*. Expression levels of the top 60 altered proteins in all samples are shown in the heat map generated by hierarchical cluster analysis (*SI Appendix*, Fig. S1), demonstrating clear differences and similarities among the groups, providing a rationale for deeper analysis.

To improve our understanding of changes in RT-induced biological processes, we also performed enrichment pathway analysis on these dysregulated proteins (with fold change >2.5) using Metascape Bioinformatics Resource (22). The results indicate that related RT-induced biological processes, such as reactive oxygen species metabolism and lysosomal pathways, were altered between the responder-IT and nonresponder-IT groups (*SI Appendix*, Fig. S2 *A* and *B*). However, different changes in biological processes were apparent in the responder-NIT and nonresponder-NIT groups, with responder-NIT showing markedly increased expression in processes associated with neutrophil degranulation and response to extracellular stimuli and nonresponder-NIT expressing increased activity in other pathways (*SI Appendix*, Fig. S3 *A* and *B*). The enrichment pathway network of responder-NIT and nonresponder-NIT determined by cluster analysis is shown in *SI Appendix*, Fig. S4 *A* and *B*.

To identify biomarkers for potential in vivo imaging probe development, we focused on membrane proteins (expression levels in all samples shown in Fig. 1*F*) that displayed significant changes. Based on a primary investigation of the functions of these proteins and the consideration of expression contrast between tumor and normal tissues, ICAM-1 was selected as a potential target for further investigation. The results of Western blot analysis and immunofluorescence staining further confirmed a higher level of ICAM-1 expression in responder-NIT compared with nonresponder-NIT (Fig. 1 *G* and *H*), consistent with the results of the proteomics analysis. Moreover, the proliferation of tumor cells was reduced in responder-NIT, as reflected by Ki67 (tumor cell proliferation index) staining (Fig. 1*H*), suggesting that ICAM-1 may be an important indicator of a local RT-induced abscopal effect. Of note, ICAM-1 overexpression was also apparent in irradiated tumors compared with control tumors (Fig. 1*F* and *SI Appendix*, Fig. S5) and was further confirmed in human tumor tissue from patients with rectal cancer or soft tissue sarcoma who underwent RT ($P < 0.05$; *SI Appendix*, Fig. S6 *A* and *B* and Table S1).

ICAM-1–Targeted Noninvasive Imaging Could Predict an RT-Induced Abscopal Effect. We next investigated whether noninvasive imaging of ICAM-1 could predict an RT-induced abscopal effect. To accomplish this, we synthesized the ICAM-1–targeted NIRF probe Dye-αICAM-1/Fab by labeling the Fab fragment of an anti–ICAM-1 antibody (αICAM-1/Fab) with DyLight800-NHS (Thermo Fisher Scientific) and obtained the PET imaging probe ^{64}Cu-NOTA-αICAM-1/Fab by conjugating αICAM-1/Fab with the chelator 1,4,7-triazacyclononanetriacetic acid (NOTA), followed by radiolabeling with ^{64}Cu (*SI Appendix*, Fig. S7). Dye-αICAM-1/Fab was confirmed to be highly pure (*SI Appendix*, Fig. S8), and the ICAM-1–targeting specificity of Dye-αICAM-1/Fab was confirmed by in vivo NIRF imaging (*SI Appendix*, Fig. S9 *A* and *B*). The purity of ^{64}Cu-NOTA-αICAM-1/Fab was determined to be >99% (*SI Appendix*, Fig. S10 *A* and *B*), and the ICAM-1 specificity of ^{64}Cu-NOTA-αICAM-1/Fab was confirmed in vitro (*SI Appendix*, Fig. S10 *C* and *D*) and in vivo (*SI Appendix*, Fig. S11 *A* and *B*).

As RT can induce ICAM-1 up-regulation in irradiated tumors (*SI Appendix*, Fig. S6 *A* and *B*), we first assessed whether the overexpressed ICAM-1 on irradiated tumors could be noninvasively detected by ICAM-1–targeted probes. RT was conducted in 4T1 tumor-bearing mice and induced strong tumor growth inhibition ($P < 0.01$; *SI Appendix*, Fig. S12 *A* and *B*), and high expression of ICAM-1 in the RT-treated tumors was visualized by NIRF imaging of Dye-αICAM-1/Fab ($P < 0.05$; *SI Appendix*, Fig. S12*C*) and small animal PET imaging of ^{64}Cu-NOTA-αICAM-1/Fab (*SI Appendix*, Fig. S12*D*). Immunofluorescence staining further confirmed ICAM-1 overexpression on the irradiated tumors, accompanied by increased CD8$^+$ cell infiltration (*SI Appendix*, Fig. S12 *E* and *F*).

Next, based on our findings regarding ICAM-1 up-regulation in responder-NIT compared with nonresponder-NIT, we hypothesized that ICAM-1–targeted imaging could be a noninvasive strategy for the prediction of an RT-induced abscopal effect. To test our hypothesis, we conducted imaging studies in mice bearing primary and secondary tumors before tumor size divergence to determine the predictive values of ICAM-1–targeted imaging for an RT-induced abscopal effect. Primary tumors of mice ($n = 14$) were irradiated, while secondary tumors were not (Fig. 2*A*). We first performed NIRF imaging of Dye-αICAM-1/Fab at 6 h postinjection (hpi) in these 14 tumor-bearing mice to noninvasively determine the expression levels of ICAM-1 in the nonirradiated tumors. Discrepant ICAM-1 expression in 14 tumors was observed by NIRF imaging (Fig. 2*B*), in which tumors with high ICAM-1 expression were also confirmed by small animal PET imaging

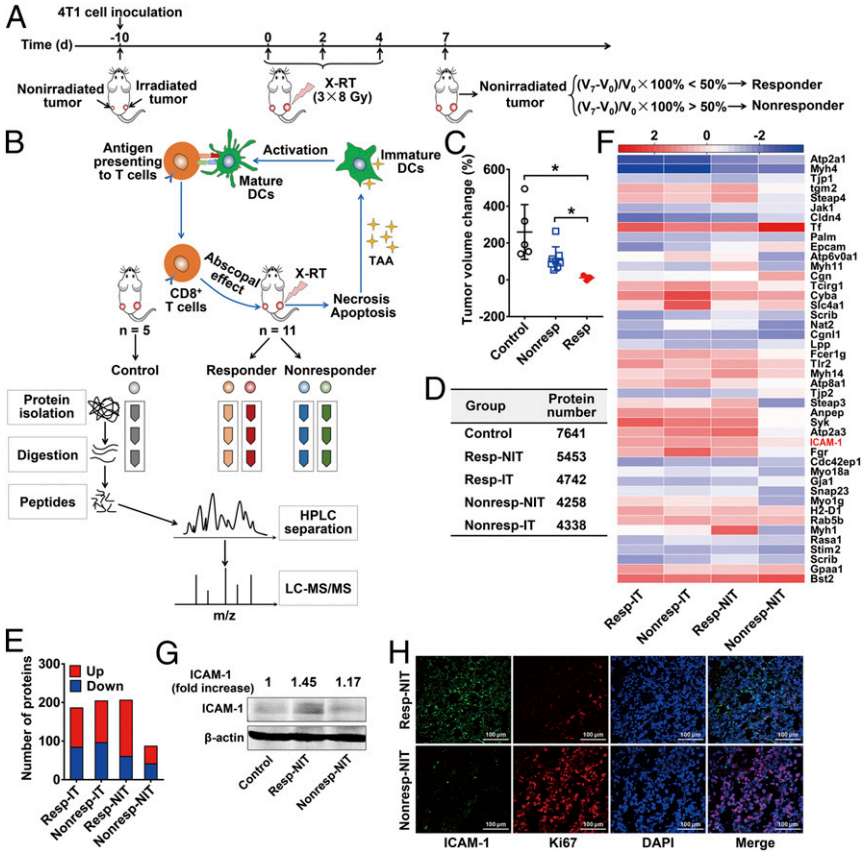

Fig. 1. Identification and validation of ICAM-1 as a biomarker in responsive nonirradiated tumors after RT. (*A*) Schedule of X-RT in 4T1 bilateral tumor-bearing mice and the definitions of responder and nonresponder mice. (*B*) Schematic view of proteomic analysis. (*C*) Grouped scatterplot presenting the change in tumor volume among nonirradiated tumors on day 7 (nonirradiated control tumors, $n = 5$; nonresponder tumors, $n = 8$; responder tumors, $n = 3$). Data are presented as mean ± SD. *$P < 0.05$, unpaired Student *t* test. (*D*) Identified protein numbers in the nonirradiated tumors of the responder group (resp-NIT), nonirradiated tumors of the nonresponder group (nonresp-NIT), irradiated tumors of the responder group (resp-IT), and irradiated tumors of the nonresponder group (nonresp-IT) by proteomic analysis. (*E*) Numbers of differently expressed proteins in each group. Red represents up-regulated expression, and blue represents down-regulated expression. (*F*) Heatmap of log2 fold change (normalized to control tumor) of 44 differentially expressed membrane proteins on day 7 in indicated groups. Data represent group mean, $n = 3$ per group. (Scale bars: white, 0; red, >2 log2 fold change; blue, <2 log2 fold change.) (*G*) Western blot analysis of ICAM-1 expression in 4T1 tumor tissues on day 7. The densities of Western blot bands were quantified by scanning densitometry with ImageJ software and are presented as the normalized fold change. (*H*) Immunofluorescence staining of ICAM-1 and Ki67 in 4T1 tumor tissues derived from resp-NIT or nonresp-NIT.

studies (Fig. 2*C*). Based on the level of ICAM-1 expression, we divided the mice into a high ICAM-1 expression group (ICAM-1 high; $n = 6$) and a low ICAM-1 expression group (ICAM-1 low; $n = 8$) and further monitored tumor growth in these two groups. Tumor growth was significantly slower in the ICAM-1 high group compared with the ICAM-1 low group ($P < 0.01$; Fig. 2*D*), suggesting that the noninvasive imaging quantification of ICAM-1 is predictive of a future RT-induced abscopal effect in the 4T1 tumor model. By contrast, compared to the control tumors without RT, RT resulted in effective inhibition of primary tumors (irradiated), while diverse tumor growth curves were observed among the nonirradiated tumors without discrimination by the ICAM-1 levels determined by noninvasive imaging (Fig. 2*E*).

Further validation in the CT26 colon carcinoma model notably showed that RT induced more intense tumor inhibition in both irradiated and nonirradiated tumors (Fig. 2*F*) than in the 4T1 tumor model when treated with the same irradiation schedule. NIRF imaging was performed, and the mice were divided into the ICAM-1 high and ICAM-1 low groups based on the fluorescence intensity of Dye-αICAM-1/Fab in the nonirradiated tumors ($P < 0.01$; *SI Appendix*, Fig. S13 *A* and *B*). Representative PET images are shown in Fig. 2*G*. Consistent with the results obtained in the 4T1 tumor model, high expression of ICAM-1 post-RT could reflect the extent of the inhibition in nonirradiated tumors ($P < 0.05$; Fig. 2*H*). Taken together, these results supported the hypothesis that increased ICAM-1 expression of nonirradiated tumors post-RT could predict the sensitivity of an antitumor abscopal response to RT.

ICAM-1–Selective Up-Regulation on Tumor-Infiltrating CD8$^+$ T Cells Plays a Vital Role in the Abscopal Effect. To elucidate the mechanisms underlying the post-RT abscopal response in tumors with high ICAM-1 expression, we first tried to identify which cell types play major roles in linking ICAM-1 expression to the abscopal effect. We confirmed the increased total membrane ICAM-1 expression in responder-NITs versus nonresponder-NITs and control tumors ($P < 0.01$; Fig. 3*A*) and identified increased ICAM-1 expression in various cell subsets, such as tumor-infiltrating immune cells, CD31$^+$ endothelial cells, and 4T1 tumor cells (Fig. 3*B*), via flow cytometry. ICAM-1 was colocalized with CD31$^+$ endothelial cells (*SI Appendix*, Fig. S14*A*), as ICAM-1 was typically expressed on endothelial cells (23). We observed that ICAM-1 was also highly expressed on CD8$^+$ cells. Importantly, the level of ICAM-1 expression on CD8$^+$ cells was significantly higher in responder-NITs compared with nonresponder-NITs and control tumors ($P < 0.05$),

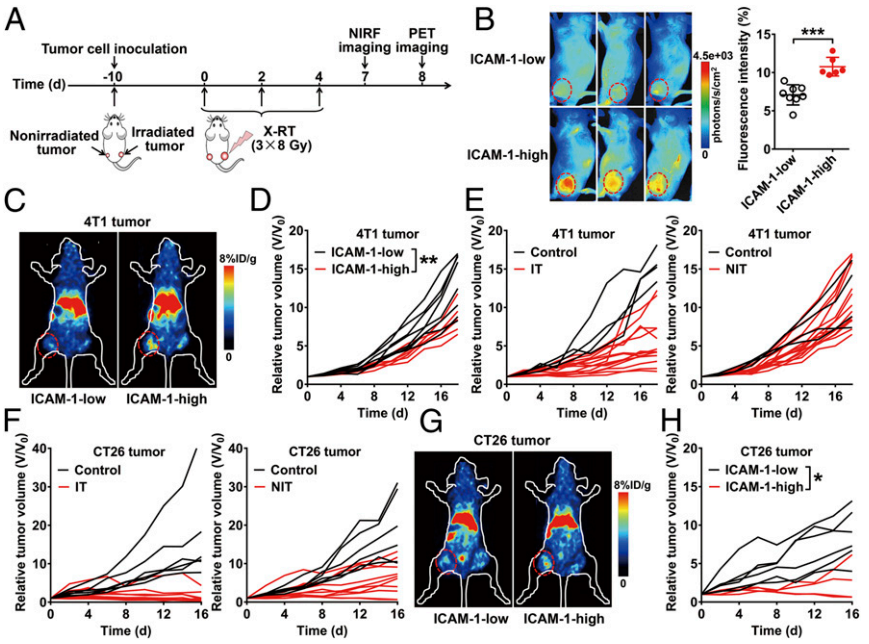

Fig. 2. Noninvasive imaging of ICAM-1 expression predicts the abscopal response to tumor RT. (*A*) Schedule of X-RT and in vivo imaging using Dye-αICAM-1/Fab or ^{64}Cu-NOTA-αICAM-1/Fab in the 4T1 or CT26 bilateral tumor-bearing mouse models. (*B*) Representative in vivo NIRF images and quantitative analysis of tumor uptake of Dye-αICAM-1/Fab at 6 hpi in 4T1 tumor-bearing mice. High or low expression of ICAM-1 was differentiated by quantitative fluorescence intensity (n = 6 to 8 per group). Data are presented as mean ± SD. ***$P < 0.001$, unpaired Student t test. (*C*) Representative small animal PET images of ^{64}Cu-NOTA-αICAM-1/Fab at 6 hpi in 4T1 tumor-bearing mice. (*D*) Growth curves of nonirradiated tumors in 4T1 tumor-bearing mice grouped (ICAM-1 high vs. ICAM-1 low) by quantitative fluorescence intensity in *B*. (*E*) Individual growth curves of the irradiated tumors (IT) and nonirradiated tumors (NIT) in the 4T1 tumor model after RT (control group, n = 4; RT group, n = 14). (*F*) Individual growth curves of the ITs and NITs in the CT26 tumor model after RT (control group, n = 6; RT group, n = 10). (*G*) Representative small animal PET images of ^{64}Cu-NOTA-αICAM-1/Fab at 6 hpi in CT26 tumor-bearing mice. (*H*) Growth curves of nonirradiated tumors in CT26 tumor-bearing mice grouped (ICAM-1 high vs. ICAM-1 low) by quantitative fluorescence intensity in *SI Appendix*, Fig. S13. Tumors are indicated by red circles. *$P < 0.05$, **$P < 0.01$, two-way ANOVA (*D* and *H*).

whereas ICAM-1 expression on the other cell subsets was comparable in the three groups (Fig. 3*B*).

To further confirm our observation, we stained the CD8$^+$ cells and found more tumor-infiltrating CD8$^+$ cells in responder-NITs than in nonresponder-NITs, in which ICAM-1 expression exhibited strong colocalization with CD8$^+$ cells (*SI Appendix*, Fig. S14*B*). In contrast, ICAM-1 expression on the vascular endothelial cells in the responder-NITs showed only slight up-regulation compared to that of the nonresponder-NITs (*SI Appendix*, Fig. S14*A*).

To further validate the role of ICAM-1 in the responses of nonirradiated tumors to RT, we blocked the expression of ICAM-1 by using an anti–ICAM-1 antibody in both 4T1 and CT26 mouse models (Fig. 3*C* and *SI Appendix*, Fig. S15*A*) and repeated the irradiation schedule. In irradiated tumors, anti–ICAM-1 blocking showed a limited effect on the abrogation of tumor inhibition by RT, as expected, because most of the growth inhibition of irradiated tumors resulted from direct cell destruction from irradiation instead of immune potentiation. In contrast, ICAM-1 blocking in nonirradiated tumors led to an almost full recovery from RT-induced tumor growth inhibition (Fig. 3*D* and *SI Appendix*, Fig. S15*B*). Additionally, CD8$^+$ T cell depletion using an anti-CD8 antibody exhibited an almost identical tumor inhibition-abrogation pattern to that of ICAM-1 blocking (Fig. 3*D* and *SI Appendix*, Fig. S15*B*). These results indicate that highly expressed ICAM-1 on CD8$^+$ cells may contribute to the responsiveness of nonirradiated tumors to RT.

In Vitro Studies Reveal the Role of ICAM-1 in Regulating the Antitumor Activity of CD8$^+$ T Cells. Based on previous reports that ICAM-1 tethers T cell and antigen-presenting cell membranes and facilitates the interaction between T cell receptors and major histocompatibility complex (MHC) molecules (24), and the fact that ICAM-1 also plays a role in sustaining longer-lasting interactions between T cells and antigen-presenting cells through the formation of immunologic synapses (25), we hypothesized that ICAM-1 facilitates the antitumor abscopal reaction by contributing to the formation of immunologic synapses. To validate this, we first stimulated splenocytes derived from wild-type mice with the TAA extracted from 4T1 tumor tissues (Fig. 3*E*). CD8$^+$ T cells were activated by exposure to TAA, as reflected in elevated interferon-γ (IFNγ) expression, in which activated CD8$^+$ T cells also showed increased ICAM-1 expression ($P < 0.0001$; *SI Appendix*, Fig. S16 *A* and *B*). Next, CD8$^+$ T cells (CD3$^+$CD8$^+$ cells) and dendritic cells (MHCII$^+$CD11c$^+$ cells) were sorted from splenocytes and lymph nodes. We pulsed the dendritic cells with TAA, followed by coculture with CD8$^+$ T cells, and observed the formation of immune synapses (*SI Appendix*, Fig. S17*A*). However, the binding of CD8$^+$ T cells and dendritic cells could be almost completely inhibited when ICAM-1 expression on the surface of CD8$^+$ T cells was blocked with an anti–ICAM-1 antibody ($P < 0.0001$; Fig. 3*F* and *SI Appendix*, Fig. S17*B*). Furthermore, the binding of ICAM-1 knockout mouse-derived CD8$^+$ T cells and dendritic cells was significantly lower than that of wild-type mouse-derived CD8$^+$ T cells and dendritic cells ($P < 0.001$; Fig. 3*G* and *SI Appendix*, Fig. S17*C*). These results indicate the importance of ICAM-1 expression on the CD8$^+$ T cells in immune synapse formation.

Cytotoxic T cells destroy tumors by relying mainly on perforin/granzyme-mediated and IFNγ-dependent pathways (26). We observed that CD8$^+$ T cells cocultured with TAA-stimulated dendritic cells highly expressed IFNγ as well as CD107a, a marker of degranulation that is a prerequisite for perforin-granzyme–mediated killing (27, 28), and that ICAM-1 blocking inhibited IFNγ production and the degranulation pathway ($P < 0.0001$; Fig. 3*H* and

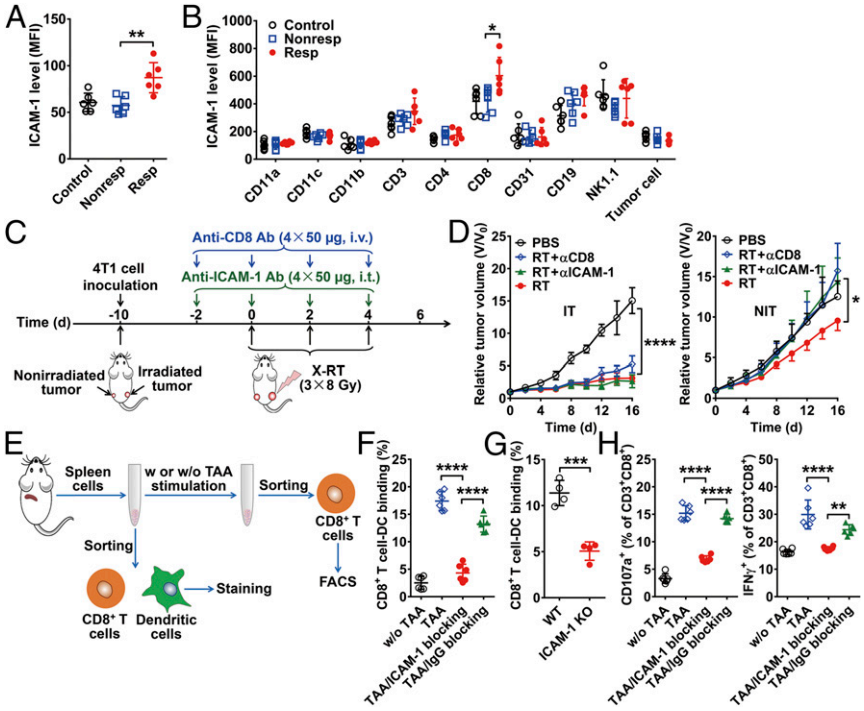

Fig. 3. Expression and functional analysis of ICAM-1. (*A*) Expression level of membrane ICAM-1 measured by flow cytometry in nonirradiated tumors ($n = 6$ per group). (*B*) Assessment of ICAM-1 expression in various cell subsets in nonirradiated tumors. Tumor cells were gated by a $CD45^-$ subset and forward scatter. (*C*) Schematic illustration of X-RT in combination with anti–ICAM-1 blocking or anti-CD8 blocking. (*D*) Tumor growth curves of irradiated tumors (IT) and nonirradiated tumors (NIT) in 4T1 tumor-bearing mice after the indicated treatments: control (PBS), RT, RT plus anti–ICAM-1 blocking (RT + αICAM-1), and RT plus anti-CD8 blocking (RT + αCD8) ($n = 5$ per group). (*E*) Schematic diagram of TAA stimulation and immune synapse formation experiments. (*F*) Flow cytometry analysis of mutual binding between $CD8^+$ T cells and dendritic cells with or without ICAM-1 blocking ($n = 6$ per group). (*G*) Flow cytometry analysis of mutual binding between wild-type or ICAM-1 knockout mouse-derived $CD8^+$ T cells and dendritic cells ($n = 4$ per group). (*H*) Flow cytometry analysis of CD107a/IFNγ expression on $CD8^+$ T cells with or without blocking with an anti–ICAM-1 antibody ($n = 6$ per group). All the numerical data are presented as mean ± SD. $^*P < 0.05$; $^{**}P < 0.01$; $^{***}P < 0.001$; $^{****}P < 0.0001$ by one-way ANOVA with Tukey's post hoc test (*A*, *B*, *F*, and *H*), two-way ANOVA (*D*), or an unpaired Student *t* test (*G*).

SI Appendix, Fig. S17*D*). In addition, knockdown of ICAM-1 expression in the OT-I $CD8^+$ T cells significantly reduced the tumor killing efficiency of B16-OVA cells ($P < 0.001$; *SI Appendix*, Fig. S18 *A* and *B*), accompanied by suppressed $CD8^+$ T cell activation (*SI Appendix*, Fig. S18*C*). Taken together, our results demonstrate that ICAM-1 not only plays a critical role in the formation of immune synapses, but also directly regulates the antitumor activity of $CD8^+$ T cells by intervening in IFNγ secretion and degranulation, constituting a potential mechanism that illustrates superior abscopal effects in tumors with high ICAM-1 expression.

Intratumoral Delivery of ICAM-1–Encoding Adenovirus to Nonirradiated Tumors Enhances the Abscopal Effect of RT. Given that RT alone is insufficient to induce ideal nonirradiated tumor inhibition and that ICAM-1 plays a critical role in $CD8^+$ T cell activation and antitumor cytotoxicity, we next sought to explore whether ICAM-1 up-regulation could bolster the abscopal antitumor responses to RT by generating ICAM-1–containing adenovirus vectors (ICAM-1 Ad) and empty control adenovirus vectors (control Ad) injected to achieve intratumoral transfection in vivo. Successful ICAM-1 transfection in vitro was confirmed by green fluorescent protein (GFP) detection (*SI Appendix*, Fig. S19 *A* and *B*). Intratumoral injection of ICAM-1 Ad into 4T1 tumors led to a significantly increased uptake of Dye-αICAM-1/Fab ($P < 0.01$; *SI Appendix*, Fig. S20*A*). Moreover, ICAM-1 Ad administration increased $CD8^+$ T cell infiltration in tumor tissues ($P < 0.05$), with minor effects on $CD4^+$ T cells (*SI Appendix*, Fig. S20*B*). This may have contributed at least partially to the improved antitumor effect of the combination of ICAM-1 Ad intratumoral injection and RT ($P < 0.01$; *SI Appendix*, Fig. S20*C*). All mice that received intratumoral ICAM-1 Ad injections showed no body weight loss (*SI Appendix*, Fig. S20*D*), suggesting tolerance to this treatment.

We next explored whether up-regulating ICAM-1 by intratumoral injection of ICAM-1 Ad into nonirradiated tumors could improve the abscopal effect of RT in the bilateral 4T1 tumor-bearing mouse model (Fig. 4*A*). RT treatment groups, including RT plus phosphate-buffered saline (PBS), RT plus control Ad, and RT plus ICAM-1 Ad, significantly inhibited the growth of irradiated tumors compared with PBS and ICAM-1 Ad only groups ($P < 0.05$; Fig. 4*B* and *SI Appendix*, Fig. S21*A*). While the effects of RT plus PBS and RT plus control Ad on growth inhibition among nonirradiated tumors were generally limited (Fig. 4*B* and *SI Appendix*, Fig. S21*B*), nonirradiated tumors intratumorally injected with ICAM-1 Ad showed a greater degree of tumor regression when combined with RT ($P < 0.001$; Fig. 4*B*).

ICAM-1 up-regulation after intratumoral ICAM-1 Ad delivery was confirmed by flow cytometry analysis ($P < 0.001$; Fig. 4*C*) and immunofluorescence staining (*SI Appendix*, Fig. S22). Additionally, we performed various flow cytometry analyses to validate improved immune cell responses among treatment groups. We observed that compared to RT plus control Ad, RT plus ICAM-1 Ad led to significantly increased tumor infiltration with $CD8^+$ T cells ($P < 0.05$), slightly decreased $CD4^+$ T cell infiltration (Fig. 4*D*), elevated IFNγ production in $CD8^+$ T cells ($P < 0.05$; Fig. 4*E*), and a significantly increased $CD8^+$-to-regulatory T (Treg) cell ratio ($P < 0.01$; Fig. 4*F*). These data support our hypothesis that ICAM-1 up-regulation in the nonirradiated tumors by intratumoral injection of ICAM-1 Ad could synergistically

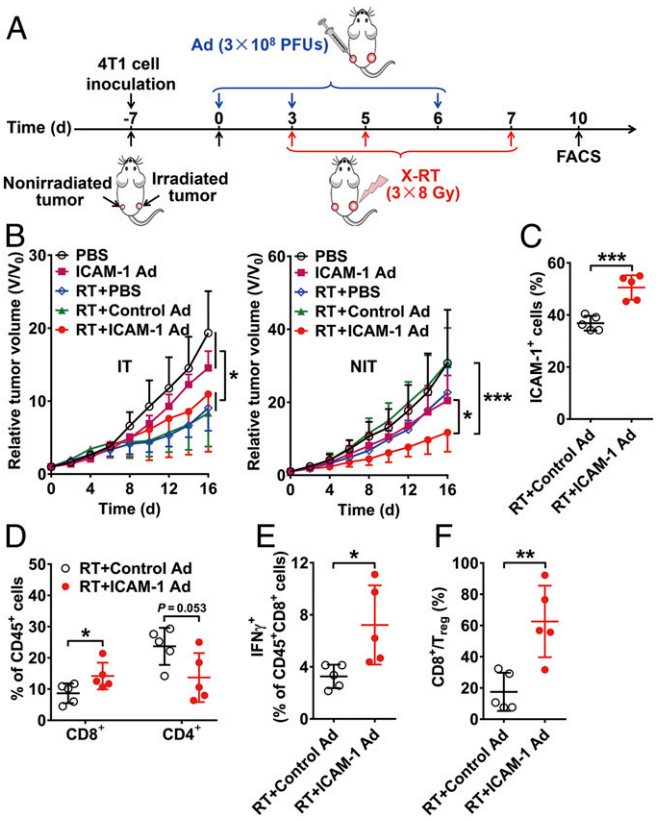

Fig. 4. Genetic up-regulation of ICAM-1 in vivo by adenovirus enhances abscopal effect of RT. (*A*) Schematic illustration of X-RT combined with ICAM-1 Ad. (*B*) Tumor growth curves of irradiated tumors (IT) and nonirradiated tumors (NIT) in 4T1 tumor-bearing mice after the indicated treatments: control (PBS), ICAM-1 expressing Ad alone (ICAM-1 Ad), RT plus PBS (RT + PBS), RT plus control Ad (RT + control Ad) or RT plus ICAM-1 expressing Ad (RT + ICAM-1 Ad) ($n = 6$ to 9 per group). (*C* and *D*) Flow cytometry analysis assessing ICAM-1$^+$ cells (*C*) and CD8$^+$/CD4$^+$ cells (*D*) in the nonirradiated tumors after the indicated treatments ($n = 5$ per group). (*E* and *F*) Flow cytometry analysis evaluating the percentage of IFNγ-secreting CD8$^+$ T cells (*E*) and the ratio of CD8$^+$/Treg cells (*F*) in nonirradiated tumors of mice after the indicated treatments ($n = 5$ per group). All the numerical data are presented as mean ± SD. *$P < 0.05$; **$P < 0.01$; ***$P < 0.001$ by two-way ANOVA (*B*) or an unpaired Student *t* test (*C*–*F*).

improve the abscopal effect induced by RT, with local elevation of ICAM-1 increasing intratumoral infiltration of activated CD8$^+$ T cells to induce immune-mediated tumor inhibition.

Imiquimod Synergizes with RT in Inhibiting the Growth of Nonirradiated Tumors by Up-Regulating ICAM-1 Expression. We next sought to investigate whether drugs that up-regulate ICAM-1 expression could be used as an adjuvant treatment with RT. Imiquimod (IMQ; also known as Aldara or R-837), an immune modulator that acts as a Toll-like receptor 7 (TLR7) agonist, was selected because studies showed it could induce significant increases in ICAM-1 levels (29, 30). To determine whether a combination of IMQ and RT could potentiate the abscopal effect, nonirradiated tumors of 4T1 tumor-bearing mice were treated with IMQ via intratumoral injection and primary tumors were subjected to RT (Fig. 5*A*). We first analyzed IMQ-treated tumors to investigate ICAM-1 up-regulation. Both Western blot ($P < 0.001$; Fig. 5*B*) and flow cytometry ($P < 0.01$; Fig. 5*C*) analyses revealed positive results. Notably, we observed that the majority of ICAM-1 expression was on CD8$^+$ T cells rather than on the tumor cells (Fig. 5*D*). Moreover, IMQ treatment led to further up-regulated ICAM-1 expression on the CD8$^+$ T cells ($P < 0.01$), in contrast to ICAM-1 expression levels in 4T1 tumor cells, which remained relatively low (Fig. 5*D*).

RT of primary tumors combined with intratumoral injection of IMQ in the nonirradiated tumors led to a significant increase in the extent of growth suppression among nonirradiated tumors compared to that of RT alone or IMQ alone in the 4T1 tumor model ($P < 0.05$; Fig. 5*E* and *SI Appendix*, Fig. S23). When blocking with anti–ICAM-1 antibody, the antitumor effect of a combination of IMQ and RT on nonirradiated 4T1 tumors was almost fully abrogated ($P < 0.05$; Fig. 5*E*). A similar effect was also observed in the CT26 tumor model (*SI Appendix*, Fig. S24). In addition, depletion of CD8$^+$ T cells in the RT plus IMQ treatment group was also able to reverse the tumor inhibition effect, while the depletion of CD4$^+$ T cells had a limited effect on reversing tumor inhibition in nonirradiated tumors (*SI Appendix*, Fig. S25 *A* and *B*). These results suggest that intratumoral IMQ administration could synergize with RT to inhibit the growth of nonirradiated tumors via an ICAM-1 and CD8$^+$ T cell-dependent manner.

We next investigated whether the change in ICAM-1 expression during IMQ treatment could be noninvasively visualized by ICAM-1–targeted NIRF and PET imaging. Markedly increased uptake of Dye-αICAM-1/Fab in the IMQ-treated tumors was observed ($P < 0.05$; Fig. 5*F*). Compared to the mice in the RT alone group, the RT plus IMQ-treated mice also exhibited significantly higher uptake of ^{64}Cu-NOTA-αICAM-1/Fab in the nonirradiated tumors ($P < 0.01$; Fig. 5*G*). Importantly, correlation analysis showed a strong negative linear correlation between tumor uptake of ^{64}Cu-NOTA-αICAM-1/Fab on day 12 and relative tumor volume changes (V_{20}/V_0) 8 d later (Pearson $r = -0.875$, $P < 0.001$; Fig. 5*H*). Hence, up-regulated ICAM-1 expression after IMQ treatment could be noninvasively detected by ICAM-1–targeted imaging, and PET imaging using ^{64}Cu-NOTA-αICAM-1/Fab could predict the growth inhibition effects of IMQ plus RT combination therapy on the nonirradiated tumors.

Systemic Delivery of IMQ by Formulated Nanoparticles Enhances the Abscopal Effects of RT. We further explored a systemic administration approach for IMQ delivery to address potential clinical limitations by encapsulating IMQ with polymeric nanoparticles fabricated with poly(lactic-coglycolic) acid (PLGA), a biocompatible polymer approved for clinical use by the US Food and Drug Administration (FDA). Polyethylene glycol (PEG) was grafted to PLGA to further increase its biocompatibility. IMQ was encapsulated by the PLGA-PEG, and the resulting PLGA-IMQ nanodrug had a well-defined spherical shape (*SI Appendix*, Fig. S26*A*), a final diameter of ~110 nm (*SI Appendix*, Fig. S26*B*), and an average electrophoretic zeta potential of −(12.03 ± 5.43) mV (*SI Appendix*, Fig. S26*C*). The encapsulation efficiency of IMQ could reach values >80%, and the encapsulated IMQ was slowly released for over 96 h, with a proportion of cumulative release of ~60% (*SI Appendix*, Fig. S26*D*).

We next investigated whether PLGA-IMQ combined with RT could have a synergistic antitumor effect on the nonirradiated tumors (Fig. 6*A*). Systemic administration of PLGA-IMQ combined with RT resulted in significantly improved inhibition of tumor growth in both nonirradiated and irradiated tumors (Fig. 6 *B* and *C*) compared with local RT, which only caused a growth delay on irradiated tumors and had limited effects on nonirradiated tumors. It is also worth noting that in vitro and in vivo toxicity studies confirmed that the PLGA-IMQ used in this study had no apparent toxicity (*SI Appendix*, Fig. S27 *A*–*D*). Immunofluorescence staining results showed significantly increased ICAM-1 expression in nonirradiated tumors from the RT plus PLGA-IMQ group compared with the RT only group ($P < 0.01$; Fig. 6 *D* and *E*), but the proliferation index of tumor cells was significantly decreased ($P < 0.0001$; Fig. 6 *D* and *E*).

To further validate the efficacy of this combination therapy strategy, we next tested the combination in a 4T1 cell stably

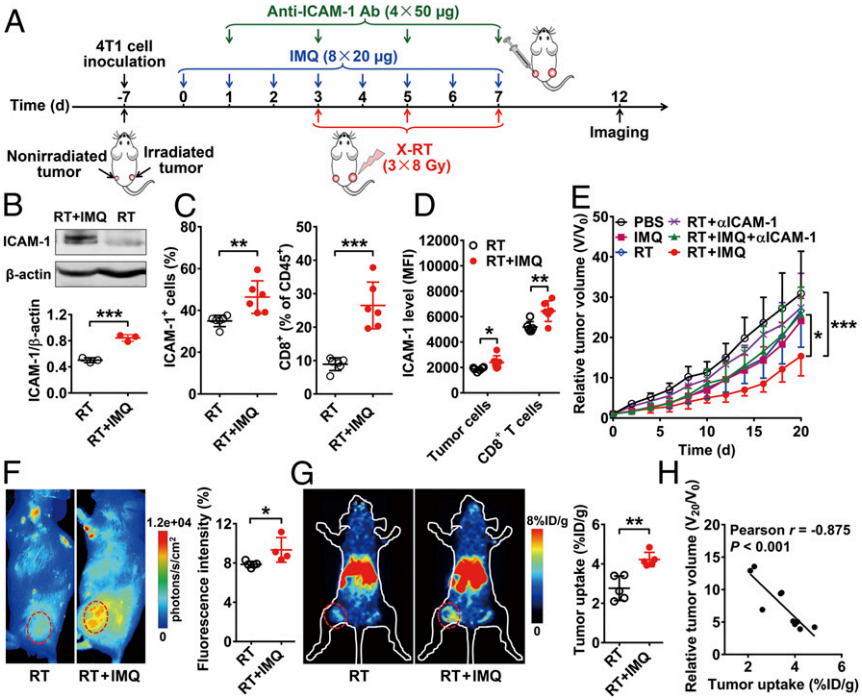

Fig. 5. IMQ-induced ICAM-1 up-regulation synergizes with local X-RT to inhibit nonirradiated tumor growth. (*A*) Schematic illustration of RT combining IMQ and in vivo imaging using Dye-αICAM-1/Fab or ^{64}Cu-NOTA-αICAM-1/Fab. (*B*) Western blot analysis of ICAM-1 expression in nonirradiated tumor tissues on day 12 after treatment with RT or RT + IMQ. Quantitative results are presented as ICAM-1/β-actin ratio ($n = 3$ per group). (*C* and *D*) Flow cytometry analysis of ICAM-1$^+$ cells and CD8$^+$ T cells (*C*) and ICAM-1 expression on CD8$^+$ cells and tumor cells (*D*) in nonirradiated tumor tissues on day 12 after treatment with RT or RT + IMQ ($n = 6$ per group). (*E*) Tumor growth curves of nonirradiated tumors in 4T1 tumor-bearing mice after the indicated treatments: control (PBS), IMQ alone (IMQ), RT alone (RT), RT plus anti–ICAM-1 blocking (RT + αICAM-1), RT plus IMQ plus anti–ICAM-1 blocking (RT + IMQ + αICAM-1), and RT plus IMQ (RT + IMQ) ($n = 6$ to 7 per group). (*F*) Representative NIRF images and quantitative analysis of tumor uptake of Dye-αICAM-1/Fab at 6 hpi in 4T1 tumor-bearing mice after treatment with RT or RT + IMQ ($n = 4$ to 5 per group). (*G*) Representative small animal PET images and quantitative analysis of tumor uptake of ^{64}Cu-NOTA-αICAM-1/Fab at 6 hpi in 4T1 tumor-bearing mice after treatment with RT or RT + IMQ ($n = 5$ per group). Nonirradiated tumors are indicated by red circles. Numerical data are presented as mean ± SD. (*H*) Correlation analysis of relative tumor volume on day 20 (V_{20}/V_0) and tumor uptake of ^{64}Cu-NOTA-αICAM-1/Fab on day 12. *$P < 0.05$; **$P < 0.01$; ***$P < 0.001$ by unpaired Student *t* test (*B–D*, *F*, and *G*), two-way ANOVA (*E*), or Pearson correlation analysis (*H*).

transfected with firefly luciferase (4T1-fLuc) tumor model bearing both subcutaneous tumor and lung metastases (*SI Appendix*, Fig. S28*A*) to mimic the clinical situation of patients with both a primary tumor and metastatic lesions (31, 32). PLGA-IMQ was administered systemically, but only subcutaneous tumors were irradiated. This combination treatment led to remarkable tumor regression in both the primary subcutaneous tumors ($P < 0.01$; *SI Appendix*, Fig. S28*B*) and the lung metastases ($P < 0.05$; Fig. 6 *F* and *G*). Additionally, body weight loss was limited in the mice in both groups (*SI Appendix*, Fig. S28*C*). Taken together, these results confirm that systemic administration of the PLGA-IMQ nanodrug enhanced the abscopal effect of RT.

Discussion

Metastasis and its related complications account for >90% of mortality from many types of cancers (33, 34). While RT is the mainstay treatment for many malignancies, its effectiveness against metastatic lesions has been limited. It has been reported that in rare instances, RT may induce an abscopal effect that inhibits metastatic lesions, indicating a potential avenue of therapeutic direction. Hence, investigating and harnessing the abscopal effects of RT with effective combination strategies (such as immunotherapy) may provide powerful tools to deal with disseminated metastases (1, 2). However, the quest for selection of the appropriate combinational therapeutics for RT and for the optimization of RT regimens (e.g., irradiation fraction and schedule) to achieve effective abscopal responses is hampered by a limited understanding of the mechanisms underlying the abscopal effect and the absence of reliable noninvasive imaging methods for its early outcome prediction (35).

The low occurrence rate of abscopal responses to RT proved challenging to investigate. To address this issue, in this study we lowered the threshold criterion for abscopal responses in murine tumor models. This proved to be conducive to our study, as we were able to gain greater insight into the early mechanisms orchestrating the abscopal effect. Our results identify ICAM-1 as a potential biomarker for predicting the effectiveness of abscopal responses to local X-ray RT (X-RT). We found that high expression of ICAM-1 was well correlated with the growth inhibition of nonirradiated tumors after RT, and that ICAM-1–targeted PET imaging is clinically promising for the noninvasive prediction of the responses of nonirradiated tumors to RT or RT combinations. Moreover, up-regulation of ICAM-1 expression by either a genetic or pharmacologic approach enhanced the abscopal effect of RT to effectively ablate the primary tumor and eliminate distant metastases.

We found that RT selectively up-regulated ICAM-1 expression on CD8$^+$ T cells but not on other types of cells in the nonirradiated tumors that are responsive to RT, consistent with previous studies showing that the abscopal effect of RT is T cell immunity-related (2). To test the validity of our results, we performed in vivo blocking of ICAM-1 and found that it fully abrogated the abscopal effect of RT, showing almost the same capability as the depletion of CD8$^+$ T cells, further confirming that the presence of ICAM-1 plays a vital role in the CD8$^+$ T cell-related abscopal response of RT. Furthermore, intratumoral injection of ICAM-1 Ad or IMQ

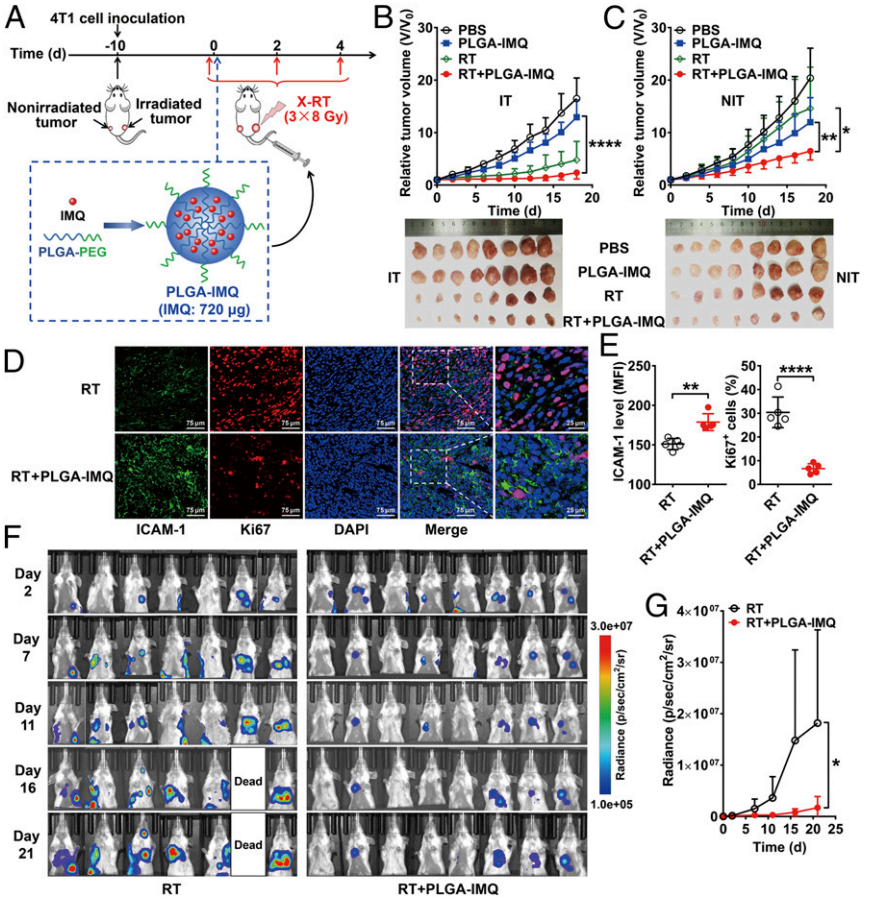

Fig. 6. Systemic delivery of IMQ by PLGA nanoparticles enhances abscopal effect of RT in mice. (*A*) Schematic illustration of the structure of PLGA-IMQ and schedule of X-RT combined with PLGA-IMQ treatment. (*B*) Tumor growth curves of irradiated tumors (IT) in 4T1 tumor-bearing mice and photographs of tumors harvested at the endpoint (below) after the indicated treatments: control (PBS), PLGA-IMQ alone (PLGA-IMQ), RT alone (RT), and RT plus PLGA-IMQ (RT + PLGA-IMQ) ($n = 8$ per group). (*C*) Tumor growth curves of nonirradiated tumors (NIT) in 4T1 tumor-bearing mice and photographs of tumors harvested at the endpoint (below) after the indicated treatments. (*D* and *E*) Immunofluorescence staining (*D*) and quantification (*E*) of ICAM-1 and Ki67 in nonirradiated tumor tissues after treatment with RT or RT + PLGA-IMQ ($n = 5$ per group). (*F* and *G*) Serial bioluminescence images (*F*) of 4T1-fLuc tumor-bearing mice after the indicated treatments: RT alone (RT) and RT plus PLGA-IMQ (RT + PLGA-IMQ) ($n = 7$ to 8 per group). Quantitative results (*G*) are presented as quantified bioluminescence signals from the lungs. Numerical data are presented as mean ± SD. $^*P < 0.05$; $^{**}P < 0.01$; $^{****}P < 0.0001$ by unpaired Student *t* test (*E*) or two-way ANOVA (*B*, *C*, and *G*).

and systemic administration of PLGA-IMQ can also significantly enhance the responses of nonirradiated tumors to RT and also can be nullified by ICAM-1 blocking and $CD8^+$ T cell depletion. Note that these treatment strategies do not selectively up-regulate ICAM-1 on $CD8^+$ T cells but may up-regulate the expression of ICAM-1 on other cells in tumor tissue. Therefore, not only is the role of ICAM-1 in the responsiveness of nonirradiated tumors to RT attributed to direct up-regulation on $CD8^+$ T cells, but its up-regulation on other cells also may contribute to the enhanced abscopal effect of combinational RT, as previous studies have demonstrated that the ICAM-1 expression by mature dendritic cells is essential to establishing a long-lasting dendritic cell–T cell interaction (36), and ICAM-1 expressed by tumor cells may lead to T cell-specific recognition and enhanced effector T cell adhesion (37). Moreover, elevated ICAM-1 expression on vascular endothelial cells may facilitate the recruitment of additional $CD8^+$ T cells to nonirradiated tumors (38, 39), as T cells express both ICAM-1 and its ligand lymphocyte function-associated antigen-1 (40), which plays a major role in interacting with ICAM-1 expressed on dendritic cells, tumor cells, and endothelial cells.

The role of ICAM-1 in the abscopal effect of RT may be attributed to two mechanisms: The up-regulation of ICAM-1 on $CD8^+$ T cells activates the antitumor function of $CD8^+$ T cells, and the up-regulation of ICAM-1 on other cells of the tumor tissue by RT combinations (e.g., IMQ used in this study) enhances the tumor infiltration and functional capacities of circulating $CD8^+$ T cells. Although further studies of the molecular mechanisms are still needed, the blocking of ICAM-1 can fully invalidate the abscopal effect of RT in tumor models treated with RT alone or RT in combination with IMQ, confirming the critical role of ICAM-1 in the responsiveness of nonirradiated tumors and substantiating that ICAM-1 can be a predictive biomarker for the abscopal effect of RT.

Early prediction and precise monitoring of the abscopal effect of RT with or without the combination of adjuvants would facilitate patient stratification and aid the design of optimal combination regimens to optimize patient outcomes. Classic methods of biomarker detection related to the abscopal effect of RT, such as biopsy followed by immunohistochemical staining, has limitations in providing accurate information due to the heterogeneity of tumors. This method also has limited value for obtaining whole-body information regarding tumor progression and is an invasive procedure that cannot be repeated frequently. In contrast, PET imaging with ^{18}F-fludeoxyglucose (^{18}F-FDG) is noninvasive and can provide quantitative whole-body information during tumor therapy in clinical settings (15, 41). However, PET imaging of ^{18}F-FDG reflects the glucose metabolism in normal and abnormal tissues, which lacks selectivity for specific biomarkers

(41). Therefore, PET imaging for specific biomarkers related to the abscopal effect of RT would allow a more precise prediction of the responses of nonirradiated metastatic lesions.

Our study shows that PET imaging of ICAM-1 expression in nonirradiated tumors could be used for predicting the responsiveness of nonirradiated tumors to RT. This noninvasive imaging strategy could be potentially implemented in clinical settings based on several key aspects. First, as the combination of RT with immunotherapy, such as checkpoint inhibitors like pembrolizumab and ipilimumab, have already been clinically used to boost the abscopal effect of RT (1, 2, 42), noninvasive monitoring of nonirradiated metastatic lesions is a key to better management of cancer patients. Although ^{18}F-FDG PET is routinely used in the clinic to monitor cancer treatments, it has significant shortcomings for immunotherapy-related treatments, because pseudoprogression during therapy often occurs due to infiltration of lymphocytes within tumors, interfering with its ability to differentiate between tumor relapse and lymphocyte infiltration-induced active antitumor effect due to a lack of specificity (43, 44). In contrast, PET imaging of ICAM-1 could be used to noninvasively visualize ICAM-1 changes after therapy, which can reflect infiltration of activated $CD8^+$ T cells, to predict the responsiveness of nonirradiated or metastatic lesions. Currently, a first in-human trial of a PET imaging probe based on ^{89}Zr-labeled anti-CD8 minibody has been reported (45), which would allow quick profiling of the infiltration of $CD8^+$ T cells in tumors after therapy. Compared to the CD8 imaging probe, which lacks information regarding $CD8^+$ T cell activation status (44, 46), the ICAM-1 imaging probe used in this study is theoretically superior, as it can accurately monitor $CD8^+$ T cell activation and function to differentiate it from the T cell exhaustion that occurs due to immune escape.

Second, as RT alone generally cannot induce effective abscopal effects, combination therapy regimens are used in the clinic to maximize the antitumor immune response induced by RT. However, selection of combinational drugs to achieve an optimal antitumor effect on both irradiated tumors and metastatic lesions at the earliest stage of combination therapy is challenging. To address this, we propose that ICAM-1–targeted PET imaging could allow for a high-throughput screening process to select potentially viable drugs to be combined with RT in preclinical animal models, as ICAM-1 expression can reflect antitumor immune fidelity, and PET imaging provides an efficient noninvasive medium, allowing for quick and simple screening for extensive amounts of therapeutics in future studies. Drugs that effect the up-regulation of ICAM-1 expression could then be identified as viable candidates for combination with RT. Noninvasive monitoring of ICAM-1 could also identify and monitor the effectiveness of combination therapeutics in a clinical setting, as ICAM-1 levels rise even at the early stage of combination therapy. Indeed, as a proof of concept, we demonstrate in this study that IMQ therapy-induced ICAM-1 up-regulation can be detected by ICAM-1–targeted PET imaging, which then allows for the detected ICAM-1 levels to provide early prediction of abscopal tumor growth inhibition. These results also explain in part several recent preclinical studies showing the synergistic effects of combining TLR7 agonists and RT for improving tumor responses (47–49).

Several recent studies have demonstrated the feasibility of radiolabeled anti–ICAM-1 antibodies for noninvasive imaging of ICAM-1 expression in vivo in animal models (50, 51). Instead of the intact antibodies used in these studies, which have low clearance in circulation and in normal organs, we selected the ICAM-1 antibody Fab fragment for probe preparation, as it is considered more clinically relevant for antibody-based imaging purposes (e.g., rapid tumor penetration, low normal organ uptake, high tumor imaging contrast). Several peptides have also been identified as specific for ICAM-1 (52, 53), and the clinical translation potential of PET imaging probes may be achieved in further studies using optimized peptides. Indeed, we are currently sponsoring an early Phase I trial (ClinicalTrials.gov identifier NCT04596670) involving noninvasive PET imaging of ICAM-1 expression using a ^{68}Ga-radiolabeled peptide in cancer patients before and after RT.

In summary, the present study demonstrates that ICAM-1 up-regulation is a potential predictive biomarker for the responsiveness of nonirradiated tumors to RT or RT combination therapies, and that ICAM-1–targeted imaging can noninvasively detect the dynamic expression of ICAM-1 levels with a promising clinical outlook. Additionally, ICAM-1 is also an attractive target for interventions to amplify the abscopal response of RT, which may allow PET imaging of ICAM-1 for the high-throughput screening of drugs that could be used in combination with RT and guide the optimization of radiation schedules and combination regimens. Furthermore, we designed and fabricated a TLR7 agonist-based nanodrug of which all components are FDA-approved. This would enable a potential clinical translation to enhance the abscopal effects of local RT toward improved systemic antitumor therapeutic outcomes.

Materials and Methods

All animal experiments were conducted according to protocols approved by the Institutional Animal Care and Use Committee at Peking University. Patient tumor samples were obtained from Peking University First Hospital and were deidentified before use in this study. Written informed consent was obtained from all patients, and all the procedures were approved by the Institutional Review Board of Peking University First Hospital. Detailed information on animal models, tumor treatments, proteomics analysis, Western blotting, preparation of imaging probes, PET and NIRF imaging, synthesis of PLGA-IMQ nanoparticles, flow cytometry, and immunofluorescence staining is provided in the *SI Appendix*.

Data Availability. All study data are included in the main text and/or *SI Appendix*.

ACKNOWLEDGMENTS. This work was supported by grants from the National Key R&D Program of China (2018YFC1313300 and 2018YFE0205300), the National Natural Science Foundation of China (81671747, 81873907, and 81920108020), the Beijing Natural Science Foundation (L172007 and JQ19026), and the Clinical Medicine Plus X-Young Scholars Project of Peking University (PKU2019LCXQ023).

1. F. G. Herrera, J. Bourhis, G. Coukos, Radiotherapy combination opportunities leveraging immunity for the next oncology practice. *CA Cancer J. Clin.* **67**, 65–85 (2017).
2. W. Ngwa *et al.*, Using immunotherapy to boost the abscopal effect. *Nat. Rev. Cancer* **18**, 313–322 (2018).
3. K. Reynders, T. Illidge, S. Siva, J. Y. Chang, D. De Ruysscher, The abscopal effect of local radiotherapy: Using immunotherapy to make a rare event clinically relevant. *Cancer Treat. Rev.* **41**, 503–510 (2015).
4. Y. Liu *et al.*, Abscopal effect of radiotherapy combined with immune checkpoint inhibitors. *J. Hematol. Oncol.* **11**, 104 (2018).
5. M. E. Rodriguez-Ruiz, I. Vitale, K. J. Harrington, I. Melero, L. Galluzzi, Immunological impact of cell death signaling driven by radiation on the tumor microenvironment. *Nat. Immunol.* **21**, 120–134 (2020).
6. M. E. Rodríguez-Ruiz, C. Vanpouille-Box, I. Melero, S. C. Formenti, S. Demaria, Immunological mechanisms responsible for radiation-induced abscopal effect. *Trends Immunol.* **39**, 644–655 (2018).
7. Y. Abuodeh, P. Venkat, S. Kim, Systematic review of case reports on the abscopal effect. *Curr. Probl. Cancer* **40**, 25–37 (2016).
8. M. A. Postow *et al.*, Immunologic correlates of the abscopal effect in a patient with melanoma. *N. Engl. J. Med.* **366**, 925–931 (2012).
9. E. B. Golden *et al.*, Local radiotherapy and granulocyte-macrophage colony-stimulating factor to generate abscopal responses in patients with metastatic solid tumours: A proof-of-principle trial. *Lancet Oncol.* **16**, 795–803 (2015).
10. C. Twyman-Saint Victor *et al.*, Radiation and dual checkpoint blockade activate non-redundant immune mechanisms in cancer. *Nature* **520**, 373–377 (2015).
11. A. B. Sharabi *et al.*, Stereotactic radiation therapy augments antigen-specific PD-1-mediated antitumor immune responses via cross-presentation of tumor antigen. *Cancer Immunol. Res.* **3**, 345–355 (2015).
12. E. D. Kwon *et al.*; CA184-043 Investigators, Ipilimumab versus placebo after radiotherapy in patients with metastatic castration-resistant prostate cancer that had progressed after docetaxel chemotherapy (CA184-043): A multicentre, randomised, double-blind, phase 3 trial. *Lancet Oncol.* **15**, 700–712 (2014).

13. E. B. Golden, S. Demaria, P. B. Schiff, A. Chachoua, S. C. Formenti, An abscopal response to radiation and ipilimumab in a patient with metastatic non-small cell lung cancer. *Cancer Immunol. Res.* **1**, 365–372 (2013).
14. S. Demaria, C. N. Coleman, S. C. Formenti, Radiotherapy: Changing the game in immunotherapy. *Trends Cancer* **2**, 286–294 (2016).
15. M. L. James, S. S. Gambhir, A molecular imaging primer: Modalities, imaging agents, and applications. *Physiol. Rev.* **92**, 897–965 (2012).
16. T. N. Ramos, D. C. Bullard, S. R. Barnum, ICAM-1: Isoforms and phenotypes. *J. Immunol.* **192**, 4469–4474 (2014).
17. H. Machelska *et al*., Opioid control of inflammatory pain regulated by intercellular adhesion molecule-1. *J. Neurosci.* **22**, 5588–5596 (2002).
18. P. J. Lindsberg, O. Carpén, A. Paetau, M. L. Karjalainen-Lindsberg, M. Kaste, Endothelial ICAM-1 expression associated with inflammatory cell response in human ischemic stroke. *Circulation* **94**, 939–945 (1996).
19. I. X. Chen *et al*., A bilateral tumor model identifies transcriptional programs associated with patient response to immune checkpoint blockade. *Proc. Natl. Acad. Sci. U.S.A.* **117**, 23684–23694 (2020).
20. R. M. Zemek *et al*., Sensitization to immune checkpoint blockade through activation of a STAT1/NK axis in the tumor microenvironment. *Sci. Transl. Med.* **11**, eaav7816 (2019).
21. B. Schrand *et al*., Radiation-induced enhancement of antitumor T-cell immunity by VEGF-targeted 4-1BB costimulation. *Cancer Res.* **77**, 1310–1321 (2017).
22. Y. Zhou *et al*., Metascape provides a biologist-oriented resource for the analysis of systems-level datasets. *Nat. Commun.* **10**, 1523 (2019).
23. C. F. Krieglstein, D. N. Granger, Adhesion molecules and their role in vascular disease. *Am. J. Hypertens.* **14**, 44S–54S (2001).
24. D. R. Fooksman *et al*., Functional anatomy of T cell activation and synapse formation. *Annu. Rev. Immunol.* **28**, 79–105 (2010).
25. N. Hogg, M. Laschinger, K. Giles, A. McDowall, T-cell integrins: More than just sticking points. *J. Cell Sci.* **116**, 4695–4705 (2003).
26. L. Martínez-Lostao, A. Anel, J. Pardo, How do cytotoxic lymphocytes kill cancer cells? *Clin. Cancer Res.* **21**, 5047–5056 (2015).
27. K. Krzewski, A. Gil-Krzewska, V. Nguyen, G. Peruzzi, J. E. Coligan, LAMP1/CD107a is required for efficient perforin delivery to lytic granules and NK-cell cytotoxicity. *Blood* **121**, 4672–4683 (2013).
28. M. R. Betts, R. A. Koup, Detection of T-cell degranulation: CD107a and b. *Methods Cell Biol.* **75**, 497–512 (2004).
29. C. Rydberg, A. Månsson, R. Uddman, K. Riesbeck, L. O. Cardell, Toll-like receptor agonists induce inflammation and cell death in a model of head and neck squamous cell carcinomas. *Immunology* **128**, e600–e611 (2009).
30. M. Z. Dewan *et al*., Synergy of topical Toll-like receptor 7 agonist with radiation and low-dose cyclophosphamide in a mouse model of cutaneous breast cancer. *Clin. Cancer Res.* **18**, 6668–6678 (2012).
31. L. Gao *et al*., Enhanced anti-tumor efficacy through a combination of integrin αvβ6-targeted photodynamic therapy and immune checkpoint inhibition. *Theranostics* **6**, 627–637 (2016).
32. C. Wang *et al*., Immunological responses triggered by photothermal therapy with carbon nanotubes in combination with anti-CTLA-4 therapy to inhibit cancer metastasis. *Adv. Mater.* **26**, 8154–8162 (2014).
33. S. Valastyan, R. A. Weinberg, Tumor metastasis: Molecular insights and evolving paradigms. *Cell* **147**, 275–292 (2011).
34. P. S. Steeg, Tumor metastasis: Mechanistic insights and clinical challenges. *Nat. Med.* **12**, 895–904 (2006).
35. Z. S. Buchwald *et al*., Radiation, immune checkpoint blockade and the abscopal effect: A critical review on timing, dose and fractionation. *Front. Oncol.* **8**, 612 (2018).
36. A. Scholer, S. Hugues, A. Boissonnas, L. Fetler, S. Amigorena, Intercellular adhesion molecule-1-dependent stable interactions between T cells and dendritic cells determine $CD8^+$ T cell memory. *Immunity* **28**, 258–270 (2008).
37. J. Turner, J. G. Rhee, D. F. Fabian, A. T. Lefor, Expression of ICAM-1 enhances in vivo lymphocyte adhesion in a murine fibrosarcoma. *J. Surg. Oncol.* **66**, 39–44 (1997).
38. E. Markovsky *et al*., An antitumor immune response is evoked by partial-volume single-dose radiation in 2 murine models. *Int. J. Radiat. Oncol. Biol. Phys.* **103**, 697–708 (2019).
39. H. Harjunpää, M. Llort Asens, C. Guenther, S. C. Fagerholm, Cell adhesion molecules and their roles and regulation in the immune and tumor microenvironment. *Front. Immunol.* **10**, 1078 (2019).
40. N. A. Zumwalde, E. Domae, M. F. Mescher, Y. Shimizu, ICAM-1-dependent homotypic aggregates regulate CD8 T cell effector function and differentiation during T cell activation. *J. Immunol.* **191**, 3681–3693 (2013).
41. L. Tagliabue, A. Del Sole, Appropriate use of positron emission tomography with [(18) F]fluorodeoxyglucose for staging of oncology patients. *Eur. J. Intern. Med.* **25**, 6–11 (2014).
42. C. Vanpouille-Box, S. C. Formenti, S. Demaria, Toward precision radiotherapy for use with immune checkpoint blockers. *Clin. Cancer Res.* **24**, 259–265 (2018).
43. Z. Xiao, A. T. Mayer, T. W. Nobashi, S. S. Gambhir, ICOS is an indicator of T-cell-mediated response to cancer immunotherapy. *Cancer Res.* **80**, 3023–3032 (2020).
44. A. Iravani, R. J. Hicks, Imaging the cancer immune environment and its response to pharmacologic intervention, Part 2: The role of novel PET agents. *J. Nucl. Med.* **61**, 1553–1559 (2020).
45. N. Pandit-Taskar *et al*., First-in-humans imaging with 89Zr-Df-IAB22M2C anti-CD8 minibody in patients with solid malignancies: Preliminary pharmacokinetics, biodistribution, and lesion targeting. *J. Nucl. Med.* **61**, 512–519 (2020).
46. P. L. Choyke, Can molecular imaging measure T-cell activation? *Cancer Res.* **80**, 2975–2976 (2020).
47. H. Chi *et al*., Anti-tumor activity of Toll-like receptor 7 agonists. *Front. Pharmacol.* **8**, 304 (2017).
48. H. Ito, Combination therapy with TLR7 agonist and radiation is effective for the treatment of solid cancer. *Ann. Transl. Med.* **4**, 95 (2016).
49. S. J. Dovedi *et al*., Systemic delivery of a TLR7 agonist in combination with radiation primes durable antitumor immune responses in mouse models of lymphoma. *Blood* **121**, 251–259 (2013).
50. M. Mosley, J. Baguña Torres, D. Allen, B. Cornelissen, Immuno-imaging of ICAM-1 in tumours by SPECT. *Nucl. Med. Biol.* **84-85**, 73–79 (2020).
51. W. Wei *et al*., Development and characterization of CD54-targeted immunoPET imaging in solid tumors. *Eur. J. Nucl. Med. Mol. Imaging* **47**, 2765–2775 (2020).
52. H. Yusuf-Makagiansar, T. J. Siahaan, Binding and internalization of an LFA-1-derived cyclic peptide by ICAM receptors on activated lymphocyte: A potential ligand for drug targeting to ICAM-1-expressing cells. *Pharm. Res.* **18**, 329–335 (2001).
53. C. Garnacho, D. Serrano, S. Muro, A fibrinogen-derived peptide provides intercellular adhesion molecule-1-specific targeting and intraendothelial transport of polymer nanocarriers in human cell cultures and mice. *J. Pharmacol. Exp. Ther.* **340**, 638–647 (2012).